

Analytical solution of crystal diffraction intensity

Wan-Li Shang(尚万里), Ao Sun(孙奥), Hua-Bin Du(杜华冰), Guo-Hong Yang(杨国洪), Min-Xi Wei(韦敏习), Xu-Fei Xie(谢旭飞), Xing-Sen Che(车兴森), Li-Fei Hou(侯立飞), Wen-Hai Zhang(张文海), Miao Li(黎淼), Jun Shi(施军), Feng Wang(王峰), Hai-En He(何海恩), Jia-Min Yang(杨家敏), Shao-En Jiang(江少恩), and Bao-Han Zhang(张保汉)

Citation: Chin. Phys. B, 2021, 30 (**11**): 116101. DOI: 10.1088/1674-1056/ac0132
Journal homepage: http://cpb.iphy.ac.cn; http://iopscience.iop.org/cpb

What follows is a list of articles you may be interested in

Hydrogen isotopic replacement and microstructure evolution in zirconium deuteride implanted by 150 keV protons

Man Zhao(赵嫚), Mingxu Zhang(张明旭), Tao Wang(王韬), Jiangtao Zhao(赵江涛), Pan Dong(董攀), Zhen Yang(杨振), and Tieshan Wang(王铁山)

Chin. Phys. B, 2021, 30 (**10**): 106104. DOI: 10.1088/1674-1056/ac29a7

Structural, magnetic, and dielectric properties of Ni-Zn ferrite and Bi_2O_3 nanocomposites prepared by the sol-gel method

Jinmiao Han(韩晋苗), Li Sun(孙礼), Ensi Cao(曹恩思), Wentao Hao(郝文涛), Yongjia Zhang(张雍家), and Lin Ju(鞠林)

Chin. Phys. B, 2021, 30 (**9**): 096102. DOI: 10.1088/1674-1056/ac0904

Formation of nano-twinned 3C-SiC grains in Fe-implanted 6H-SiC after 1500-℃ annealing

Zheng Han(韩铮), Xu Wang(王旭), Jiao Wang(王娇), Qing Liao(廖庆), and Bingsheng Li(李炳生)

Chin. Phys. B, 2021, 30 (**8**): 086107. DOI: 10.1088/1674-1056/abff43

Characterization, spectroscopic investigation of defects by positron annihilation, and possible application of synthesized PbO nanoparticles

Sk Irsad Ali, Anjan Das, Apoorva Agrawal, Shubharaj Mukherjee, Maudud Ahmed, P M G Nambissan, Samiran Mandal, and Atis Chandra Mandal

Chin. Phys. B, 2021, 30 (**2**): 026103. DOI: 10.1088/1674-1056/abd2a9

High pressure x-ray diffraction techniques with synchrotron radiation

Jing Liu(刘景)

Chin. Phys. B, 2016, 25 (**7**): 076106. DOI: 10.1088/1674-1056/25/7/076106

Analytical solution of crystal diffraction intensity*

Wan-Li Shang(尚万里)[1], Ao Sun(孙奥)[1], Hua-Bin Du(杜华冰)[1], Guo-Hong Yang(杨国洪)[1], Min-Xi Wei(韦敏习)[1,‡], Xu-Fei Xie(谢旭飞)[1], Xing-Sen Che(车兴森)[1], Li-Fei Hou(侯立飞)[1], Wen-Hai Zhang(张文海)[1], Miao Li(黎淼)[2,†], Jun Shi(施军)[3], Feng Wang(王峰)[1], Hai-En He(何海恩)[1], Jia-Min Yang(杨家敏)[1], Shao-En Jiang(江少恩)[1], and Bao-Han Zhang(张保汉)[1]

[1] *Research Center of Laser Fusion, China Academy of Engineering Physics, Mianyang* 621900, *China*
[2] *College of Optoelectronic Engineering, Chongqing University of Posts and Telecommunications, Chongqing* 400065, *China*
[3] *Key Laboratory of Optoelectronic Technology and Systems of the Education Ministry of China, Chongqing University, Chongqing* 400030, *China*
[4] *Research Center of Laser Fusion, China Academy of Engineering Physics, Mianyang* 621900, *China*

(Received 20 January 2021; revised manuscript received 12 May 2021; accepted manuscript online 14 May 2021)

Plasma density and temperature can be diagnosed by x-ray line emission measurement with crystal, and bent crystals such as von Hamos and Hall structures are proposed to improve the diffraction brightness. In this study, a straightforward solution for the focusing schemes of flat and bent crystals is provided. Simulations with XOP code are performed to validate the analytical model, and good agreements are achieved. The von Hamos or multi-cone crystal can lead to several hundred times intensity enhancements for a 200 μm plasma source. This model benefits the applications of the focusing bent crystals.

Keywords: crystal diffraction, analytic method, x-ray diffraction

PACS: 61.05.cp, 63.20.−e, 87.10.Ca **DOI:** 10.1088/1674-1056/ac0132

1. Introduction

X-ray line emission diagnostics have provided tremendous insights into the dynamics of inertial confinement fusion (ICF), high energy density physics (HEDP), and astrophysics, such as hot-spot density and temperature profiles in ICF, plasma heating and absorption properties investigation in HEDP, as well as opacity measurements and radiation transport in astrophysics.[1–6] The first electron temperature (T_e) measurement in the national ignition facility (NIF) hohlraum was undertaken by using Mn–Co x-ray line emission spectroscopy, to test the particle and energy transport physics in a laser-driven x-ray cavity.[7] The time evolution of many physical phenomena can be investigated by measuring the x-ray line emission characteristics of high ionized plasma, with the help of streak camera, such as the x-ray absorption and diffraction process in ionized plasma.[8]

In order to investigate the x-ray line emission of plasma, crystal is utilized as the x-ray optic element for Bragg diffraction.[9,10] The flat crystal is the most conventional crystal structure and is widely used in the x-ray line emission experiments. However, the low diffraction efficiency of the flat crystal leads to an inherent problem of weak brightness and low signal-to-noise ratio, especially for the weak x-ray line emissions in experiments.

The bent crystal x-ray diffraction was firstly proposed in the 1970s.[11] To improve the experimental x-ray diffraction intensity, Hall proposed a new focusing scheme with a conically bent crystal having high collection efficiency compared with the flat crystal.[12] Another high diffraction efficiency crystal geometry, von Hamos crystal that is cylindrically bent along the non-dispersive axis was reported, and a zinc von Hamos spectrometer using a crystal made from highly oriented pyrolytic graphite to measure x-ray spectra in the 7–10 keV range has been used on a ten inch manipulator for the Omega and OmegaEP target chambers.[13] Recently, a new multi-cone x-ray imaging Bragg crystal was introduced, based on the advantages of high collection efficiency as well as good combination with a streak camera or gated strip detector.[14]

Various diffraction theories for all kinds of crystal have been developed. According to the Ewald–Laue theory for a perfect crystal, a wave field in the crystal was expressed by a Bloch function.[15] An x-ray dynamical theory of x-ray diffraction for a distorted crystal were deduced from the Maxwell equations, and a solution using the Riemann function was given.[16] Moreover, Sánchez del Río *et al.* reported the theory of Zachariasen for flat crystals, the multi-lamellar approximation for bent crystals, the Penning–Polder approximation for bent Laue crystals, and the finite difference method to calculate the diffraction profile consists in solving the Takagi–Taupin equations.[17] Mosaic crystals were considered to be formed by a large number of small perfect crystallites of microscopical or submicroscopical size which are oriented al-

*Project supported by the National Natural Science Fundation of China (Grant Nos. 11775203 and 12075219) and the China Academy of Engineering Physics (CAEP) Foundation (Grant No. CX20210019).

†Corresponding author. E-mail: limiao@cqupt.edu.cn
‡Corresponding author. E-mail: wmx17@sina.com

© 2021 Chinese Physical Society and IOP Publishing Ltd

most but not exactly, parallel to one another, and the crystallites in a mosaic crystal can be analyzed efficiently with a Monte–Carlo method.[18] The above descriptions can be numerical calculated with the widely used XOP code.[19]

However, there is no straightforward solution for the x-ray diffraction brightness in the applications of focusing bent crystals, although the complicated numerical simulations can be performed to obtain the focusing effects. In this paper, a simple model is proposed to solve the x-ray diffraction intensity of the flat, von Hamos, and multi-cone crystals. In addition, this model can be utilized to design the von Hamos and multi-cone crystals, to obtain the relevant diffraction intensities. The little limitation of our model is that the crystal reflectivity spread is not taken into consideration. The point and surface source hypothesises are taken into consideration, and the effect induced by the image size is corrected.

2. Point source hypothesis

Figure 1 illustrates the x-ray imaging properties of the flat crystal with an incident angle θ, for the case, where the distance between the point source S and the crystal's nodal line is R, the distance from the point source to the detector plane is L, and the image is at a distance z from the crystal's nodal line.

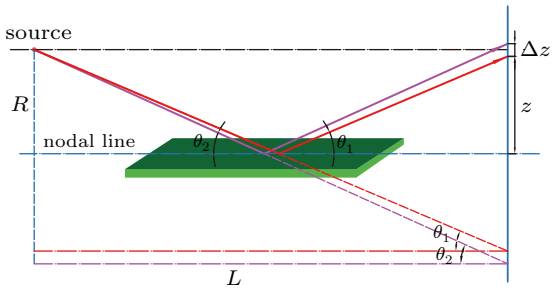


Fig. 1. X-ray imaging geometry for a flat crystal (point source).

By inspection of Fig. 1, we find the following two relations for the Bragg angle θ:

$$\tan\theta_1 = \frac{R+z}{L}, \quad \tan\theta_2 = \frac{R+z+\Delta z}{L}, \tag{1}$$

and $\mathrm{d}\theta/\mathrm{d}z = \cos^2\theta/L$ can be obtained from Eq. (1).

Then, within a single pixel (size $a\times a$) on the detector plane, the divergence angle along the spectral direction is

$$a\lim_{\Delta z\to 0}\frac{\int \sin\theta\,\mathrm{d}\theta}{\Delta z} = a\frac{\mathrm{d}\cos\theta}{\mathrm{d}z} = a\sin\theta\frac{\mathrm{d}\theta}{\mathrm{d}z} = \frac{a\sin\theta\cos^2\theta}{L}.$$

In the spatial direction, a single pixel on the detector plane has the divergency angle of $a/(2R)$. As a result, a pixel on the detector plane has the solid angle of $\frac{a^2\sin\theta\cos^2\theta}{2LR}$. The point source intensity is assumed to be I_0 (W/Sr), the crystal diffraction efficiency is η, and the detector respond is ϕ, thus the signal intensity on the detector plane is

$$I_{\mathrm{flat}} = \frac{I_0\eta\phi a^2\sin\theta\cos^2\theta}{2LR}. \tag{2}$$

As for the von Hamos crystal shown in Fig. 2, similar expressions with Eq. (1) can be found

$$\tan\theta_1 = \frac{R}{x}, \quad \tan\theta_2 = \frac{R}{x+\frac{1}{2}\Delta x} \tag{3}$$

and $\mathrm{d}\theta/\mathrm{d}x = \sin^2\theta/R$ can be obtained from Eq. (3).

Set $f(x) = \theta = \arctan(x/R)$, and then

$$\lim_{\frac{1}{2}\Delta x\to 0}\frac{\theta_2-\theta_1}{\frac{1}{2}\Delta x} = f'(x) = \lim_{\frac{1}{2}\Delta x\to 0}\frac{f(x+\frac{1}{2}\Delta x)-f(x)}{\frac{1}{2}\Delta x} = 2\frac{\Delta\theta}{\Delta x},$$

$$\lim_{\frac{1}{2}\Delta x\to 0}\frac{\cos\theta_2-\cos\theta_1}{\Delta x} = \frac{\mathrm{d}\cos\theta}{\mathrm{d}x}\frac{\Delta\theta}{\Delta x} = \frac{\sin\theta}{2}\frac{\Delta\theta}{\Delta x} = \frac{\sin^3\theta}{2R}.$$

So within a single pixel on the detector plane, the divergence angle along the spectral direction is $a\frac{\sin^3\theta}{2R}$. It should be pointed out that the divergence angle in the spatial direction depends on the divergence angle of the von Hamos cone as shown in Fig. 2, which is ψ. Then the signal intensity on the detector plane can be written as

$$I_{\text{von Hamos}} = \frac{I_0\eta\phi a\psi\sin^3\theta}{2R}. \tag{4}$$

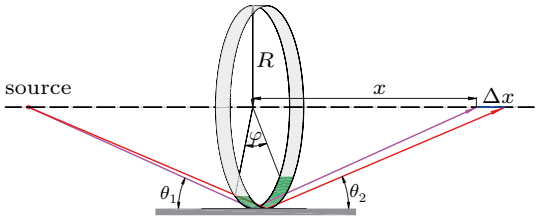


Fig. 2. X-ray imaging geometry for a von Homas crystal (single cone and point source).

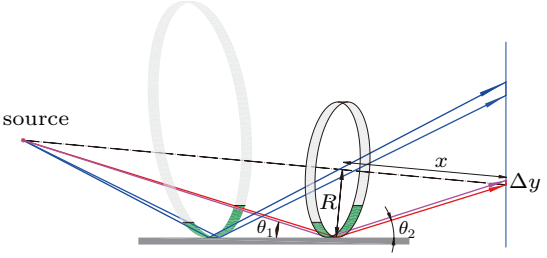


Fig. 3. X-ray imaging geometry for a multi-cone crystal (single cone and point source).

For the multi-cone crystal presented in Fig. 3, within a single pixel on the detector plane, the divergence angle along the spectral direction is the same with that of the flat crystal, and the divergence angle along the spatial direction is the same with that of the von Homas crystal. Then the signal intensity on the detector plane is

$$I_{\text{multi-cone}} = \frac{I_0 \eta \phi a \psi \sin\theta \cos^2\theta}{L}. \tag{5}$$

3. Surface source hypothesis

The surface source is assumed to be monochromatic with radius r, the total intensity is I_0, and I' is the angular distribution of the energy emitted by the surface source, thus $I_0 = \int I' \mathrm{d}s$. It should be pointed out that the source radius $r \gg a$ with a as the pixel size on the recording plane.

In the flat crystal case shown in Fig. 4, the image length on the detector plane in the spatial direction is independent of the source size r, because the crystal size is much bigger than the source size r. The image length in the spectral direction on the plane is $2r/\cos\theta$. Since the crystal reflectivity spread is not taken into consideration, the incident x-ray intensity in Δy along the spatial direction on the detector plane is $\int I' \frac{\sin\theta\cos^2\theta}{L} \frac{\Delta y}{2R} \mathrm{d}s$. According to Eq. (2), the brightness on the detector plane is

$$I_{\text{flat}} = \frac{\eta\phi \int I' \dfrac{\sin\theta\cos^2\theta}{L} \dfrac{\Delta y}{2R} \mathrm{d}s}{\dfrac{2r}{\cos\theta}\Delta y} = \frac{I_0 \eta \phi \sin\theta \cos^3\theta}{4RrL}. \tag{6}$$

In the von Hamos case shown in Fig. 5, the image area on the detector plane is $\pi r^2/\sin\theta$, and the incident x-ray intensity is $\int I' \frac{\psi \sin^3\theta}{2R} \mathrm{d}s$. As a result, according to Eq. (4), the brightness on the detector plane is

$$I_{\text{von Hamos}} = \frac{I_0 \eta \phi \psi \sin^4\theta}{2\pi R r^2}. \tag{7}$$

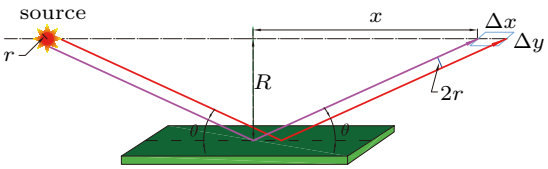


Fig. 4. X-ray imaging geometry for a flat crystal (surface source).

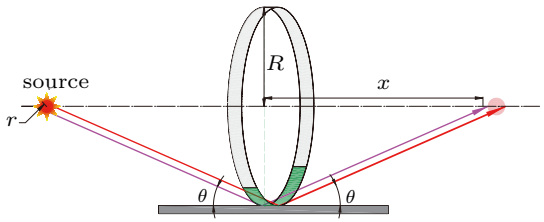


Fig. 5. X-ray imaging geometry for a von Homas crystal (single cone and surface source).

In the multi-cone case shown in Fig. 6, the image area on the detector plane is $\pi r^2/\cos\theta$, and the incident x-ray intensity is $\int I' \frac{\psi \sin\theta\cos^2\theta}{L} \mathrm{d}s$. As a result, according to Eq. (5), the brightness on the detector plane is

$$I_{\text{multi-cone}} = \frac{I_0 \eta \phi \psi \sin\theta \cos^3\theta}{\pi L r^2}. \tag{8}$$

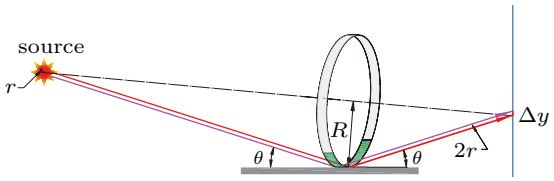


Fig. 6. X-ray imaging geometry for a multi-cone crystal (single cone and surface source).

4. Image size correction

In the application of flat or multi-cone crystal, the position of the detector plane is usually changed to obtain high spectral resolution, wide spectral region, or high focusing intensity. The crystal does not have to be in the center of the source and detector plane. Therefore, the intensity deviation on the detector plane owing to the crystal movement and image size change has to be considered. As can be seen in Fig. 7, we can find

$$\frac{z}{\tan\theta} + \frac{R}{\tan\theta} = L.$$

Then the image size on the detector plane is

$$\pi r^2 \left(\frac{z}{R}\right)^2 = \pi r^2 \left(\frac{L}{R}\tan\theta - 1\right)^2. \tag{9}$$

According to Eq. (6), the brightness on the detector plane in the flat crystal diffraction is

$$I_{\text{flat}} = \frac{I_0 \eta \phi \sin\theta \cos^3\theta}{4RrL\left(\dfrac{L\tan\theta}{R} - 1\right)^2}. \tag{10}$$

According to Eq. (8), the brightness on the detector plane in the multi-cone crystal diffraction is

$$I_{\text{multi-cone}} = \frac{I_0 \eta \phi \psi \sin\theta \cos^3\theta}{\pi L r^2 \left(\dfrac{L\tan\theta}{R} - 1\right)^2}. \tag{11}$$

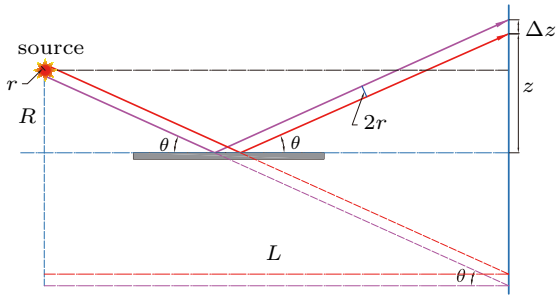


Fig. 7. X-ray imaging geometry for a flat crystal for image size correction.

5. Discussion

The von Homas and multi-cone crystals are utilized to replace the conventional flat crystal owing to the high x-ray focusing property. Here, the ratio of the diffraction intensity of the von Hamos crystal to that of the flat crystal can be achieved with Eqs. (7) and (10) as

$$\frac{I_{\text{von Hamos}}}{I_{\text{flat}}} = \frac{2L\psi\tan^3\theta}{\pi r}. \tag{12}$$

The ratio of the diffraction intensity of the multi-cone crystal to that of the flat crystal can be achieved with Eqs. (11) and (10) as

$$\frac{I_{\text{multi-cone}}}{I_{\text{flat}}} = \frac{4\psi R}{\pi r}. \tag{13}$$

Given the spectrometer parameters at the Shenguang-III (SG-III) protype laser facility, the radish R of the von Hamos crystal is 11 cm, the distance from the plasma source to the detector plane $L = 28.3$ cm, the incident Bragg angle $\theta = 38°$ for titanium (Ti) He-β line emission (4.75 keV), and the cone divergence angle $\psi = 0.55$ rad. The α-quartz crystal is adopted and $2d = 0.4256$ nm. The source size dependent intensity ratios of $I_{\text{multi-cone}}/I_{\text{flat}}$ and $I_{\text{von Hamos}}/I_{\text{flat}}$ are calculated and demonstrated in Fig. 8, and a small plasma source leads to a great focusing brightness. The effects of reflectivity spread and mosaic structure are neglected in the model.

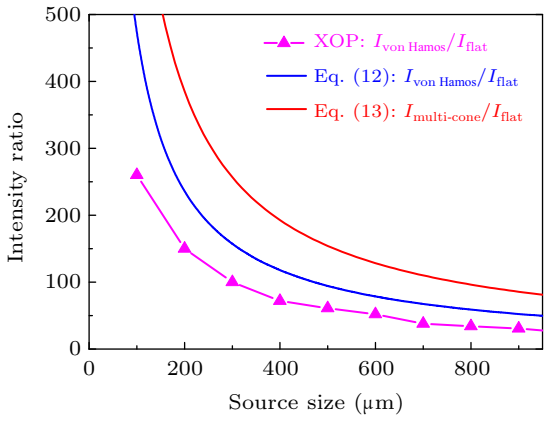


Fig. 8. Source size dependent image intensity of analytical model and simulation data of XOP.

To test the above model, we have applied computer simulations. The code XOP, a widely used public domain software for ray-tracing x-ray optics was used.[19] The simulation data are also shown in Fig. 8. The round source is set from 100 μm to 1000 μm, and the von Hamos crystal of SG-III protype laser facility is adopted, the crystal reflectivity is considered and the mosaic effect is neglected. As shown in Fig. 8, the same trend have been achieved between the analytical and simulated data. The crystal reflectivity spread is calculated in the XOP simulations, and not considered in the analytical model. This leads to the small discrepancy in Fig. 8. In the future experimental applications, the mosaic structure spread should be considered as well.[20,21]

6. Conclusion

This work gives a straightforward solution for the focusing scheme of the flat, von Hamos, and multi-cone crystals. The point source and surface source hypothesises are considered, and the image size effect to the brightness on the detector plane is corrected. This work helps the understanding of the focusing scheme of bent crystals as well as the experimental data analysis and spectrometer design.

Data availability

The data that support the findings of this study are available from the corresponding author upon reasonable request.

References

[1] Lindl J D, Amendt P, Berger R L, Glendinning S G, Glenzer S H, Haan S W, Kauffman R L, Landen O L and Suter L J 2004 *Phys. Plasmas* **11** 339
[2] Renner O and Rosmej F B 2019 *Matter Radiat. Extremes* **4** 024201
[3] Joshi T R, Hakel P, Hsu S C, Vold E L, Schmitt M J, Hoffman N M, Rauenzahn R M, Kagan G, Tang X Z, Mancini R C, Kim Y and Herrmann H W 2017 *Phys. Plasmas* **24** 056305
[4] Zhang J and Chang T 2004 *Fundaments of the Targets Physics for Laser Fusion* (Beijing: National Defence Industry)
[5] Shang W L, Betti R, Hu S X, Woo K, Hao L, Ren C, Christopherson A R, Bose A and Theobald W 2017 *Phys. Rev. Lett.* **119** 195001
[6] Shang W L , Stoeckl C, Betti R, Regan S P, Sangster T C, Hu S X, Christopherson A, Gopalaswamy V, Cao D, Seka W, Michel D T, Davis A K, Radha P B, Marshall F J, Epstein R and Solodov A A 2018 *Phys. Rev. E* **98** 033210
[7] Barrios M A, Moody J D, Suter L J, Sherlock M, Chen H, Farmer W, Jaquez J, Jones O, Kauffman R L, Kilkenny J D, Kroll J, Landen O L, Liedahl D A, Maclaren S A, Meezan N B, Nikroo A, Schneider M B, Thorn D B, Widmann K and Pérez-Callejo G 2018 *Phys. Rev. Lett.* **121** 095002
[8] Missalla T, Uschmann I and Forster E 1999 *Rev. Sci. Instrum.* **70** 1288
[9] Regan S P, Epstein R, Hamme B A, Suter L J, *et al.* 2013 *Phys. Rev. Lett.* **111** 045001
[10] Regan S P, Epstein R, Hammel B A, *et al.* 2012 *Phys. Plasmas* **19** 056307
[11] Schollmeier M S and Loisel G P 2016 *Rev. Sci. Instrum.* **87** 123511
[12] Hall T A 1984 *J. Phys. E* **17** 110
[13] Jarrott L C, Wei M S, McGuffey C, Beg F N, Nilson P M, Sorce C, Stoeckl C, Theoboald W, Sawada H, Stephens R B, Patel P K, McLean H S, Landen O L, Glenzer S H and Doppner T 2017 *Rev. Sci. Instrum.* **88** 043110
[14] Bitter M, Hill K W, Gao L, Efthimion P C, Delgado-Aparicio L, Lazerson S and Pablant N 2016 *Rev. Sci. Instrum.* **87** 11E333
[15] Takagi S and Wills H H 1962 *Acta Cryst.* **15** 1311
[16] Takagi S 1969 *J. Phys. Soc. Jpn.* **26** 1239
[17] del Río M S, Ferrero C and Mocella V 1997 *Proc. SPIE.* **3151** 312
[18] del Río M S, Bernsto S, Savoia A and Cerrina F 1962 *Rev. Sci. Instrum.* **63** 932
[19] del Río M S and Dejus R J 2011 *Proc. SPIE.* **8141** 814115
[20] Harding E C, Ao T, Bailey J E, Loisel G, Sinars D B, Geissel M, Rochau G A and Smith I C 2015 *Rev. Sci. Instrum.* **86** 043504
[21] Wang X J, Hu Z H and Wang Y N 2020 *Phys. Rev. E* **101** 043203